Energy and Fuels, Volume 30, Issue 12, 2016. pp. 10809-10822
DOI:10.1021/acs.energyfuels.6b01457

Combustion behaviour of relatively large pulverised biomass particles at rapid heating rates

Chinsung Mock[a], Hookyung Lee[b], Sangmin Choi[b], Vasilije Manovic[a,*]

[a] Centre for Combustion and Carbon Capture and Storage, Cranfield University, Cranfield, Bedfordshire MK43 0AL, United Kingdom

[b] Department of Mechanical Engineering, Korea Advanced Institute of Science and Technology (KAIST), Daehak-ro, Yuseong-gu, Daejeon, South Korea.

Corresponding author: V. Manovic, Email: v.manovic@cranfield.ac.uk, Tel: +44(0)1234 754649

Abstract

A pulverised solid fuel particle in a hot gas stream appears to have different characteristic behaviours at several stages, including heat-up, release of volatile matter, gas phase and solid combustion. The characteristics of these stages may vary distinctly depending on devolatilisation rate, the particle temperature history and its chemical and physical properties. Biomass particles manifest different combustion behaviour from that of burning coal particles under the same combustion conditions because they contain more volatiles (less fixed carbon), and they have a relatively lower particle density due to their fibrous structure. This paper presents an experimental study of burning behaviour of different types of biomass particles (torrefied wood, coffee waste and sewage sludge). The main experimental parameters—gas temperatures of 1,090 K and 1,340 K, and O_2 concentrations ranging from 10% to 40%—were employed to investigate the burning of biomass through a direct-observation approach using a high-speed photography technique at 7,000 frames/s. In the case of firing/co-firing, biomass particles must be larger than the coal particles in order to

achieve an equivalent thermal balance due to the higher energy density of coal. Therefore, the selected biomass samples were in the size range from 150–215 μm to 425–500 μm. The experimental setup has a cross-flow configuration for particle injection in order to enhance interaction between the particle and the two different streams—a cold carrier gas at 298 K, and upward-flowing post-combustion gases. It is believed that the employed experimental conditions are similar to those in a realistic furnace with a rapid heating rate of 10^5 K/s. The experimentally significant results, including the effective radii of the volatile flames, degrees of flame intensity and the maximum size of a particle are important for validation of models of single biomass particle combustion.

Introduction

Single solid fuel particles have been researched for several decades in an attempt to gain a fundamental understanding of their combustion behaviour. When a particle is exposed to a hot gas stream and a rapid heating rate, it immediately undergoes a rapid temperature increase prior to the release of volatile matter with its initial ignition [1–4]. These thermal decomposition and combustion stages are determined by environmental conditions and the physical structure of the solid particle in relation to its chemical composition [5–7]. In particular, pulverised particles are expected to burn rapidly in industrial furnaces [8, 9] however, particles of this size tend to have inconsistent flame structures and at low heating rates. Observation of these burning particles under rapid heating to high temperature, along with their flame structures and time durations of devolatilisation and combustion, would not be a simple task. Biomass has a great potential as a CO_2-neutral, low-emission energy source of heat and electricity through various applications such as combustion and gasification [10, 11]. However, biomass particles have high compositional variability, a fibrous nature and an irregular shape. They also contain highly volatile matter and are of low particle density. These

physical and chemical differences from coal result in dissimilar thermal conversion and characteristic combustion behaviour during the early stages; compared with coal, biomass combustion can offer a faster reaction rate, non-uniform gas-evolution profile and longer volatile-combustion duration [12–14]. However, these kinetic behaviours with flame structures may be inconsistent for different types of biomass and solid waste fuel due to large variation in their physical structures and chemical compositions. The different volatile flames of each biomass type influence the operating efficiency of their applications because of diverse quantities of radiant energy, dominated by flame size and luminosity.

The size of a biomass particle in pulverised combustion is expected to be larger than that of a coal particle because of low particle density and faster devolatilisation rate and, the biomass particles will not be pulverised to the same size as coal particle due to different milling behaviour and non-economic pre-processing [11, 15]. The increase of particle size is likely to enhance the ignition delay and quantity of partly unburned residue compared with a small volume of coal [16, 17] in an identical environment. Combustion behaviour is attributed to particle-size distribution and enhanced oxygen concentration as well as combustion temperature. In practical applications, solid particles are generally entrained perpendicularly into a hot gas stream along with a carrier gas at a rapid heating rate of 10^4–10^5 K/s [18]. This experiment examines biomass particles under analogous operating conditions, so as to explicitly identify the temporal variations in the burning behaviour of each particle. This is capable of accurately describing combustion processes while gaining a fundamental understanding of each burning biomass particle.

A number of previous experimental observations of particle combustion have been performed using different approaches to investigate ignition delay, kinetics and burnout time [19–22]. McLean et al. [19] introduced direct observation of an early stage of combustion, capturing

the burning particle at high gas temperature. This result gave basic evidence of the physical phenomena associated with pulverised coal combustion, such as the development of a radiative volatile flame. Khatami et al. [20] observed combustion behaviour in a quiescent environment and found that biomass has a spherical flame envelope with low luminosity and that the durations of volatile and char combustion decreased with increase in oxygen concentration due to the higher temperatures of the burning particles. Yin et al. [21] also captured informative images of spherical and cylindrical biomass particles to investigate their characteristic behaviour. Although these experimental observations have provided an acceptable fundamental understanding of fuel particles, the combustion of a single biomass particle has yet to be observed, which would provide an outline of the processes of volatile combustion and burnout as well as overlapping combustion. Thus, there is a lack of insight into the combustion behaviour of biomass in pulverised combustion due to the unclear physical structures of the volatile flame. In addition, previous research has rarely focused on the sequential combustion stages of pulverised biomass with quantitative analysis. In the present study, the determination of the optimal burning conditions of pulverised biomass particles is first attempted at a rapid heating rate under a cross-flow configuration. This layout enables a distinct description of the burning particle that is displaced along with the development of its volatile flame structure as a function of time. In addition, the maximum size of a particle that can be burned completely without dropping to the bottom of the reactor is determined from the interaction between the particle and the two perpendicular streams. Consequently, an explanation of burning particles at these environmental conditions with measured values could support development of a mathematical model of a single biomass particle.

Experimental Setup

Particle samples and separation

The biomass samples prepared for the experimental work include torrefied wood, coffee waste and sewage sludge, as shown in Fig. 1. Torrefied wood was thermally treated in a gas temperature environment of 573 K. The thermal treatment converts oxygen to CO and CO_2 while increasing energy density and hydrophobicity. This torrefied particle contains less volatile matter and relatively more fixed carbon than the raw particle. Coffee waste is the residue of an extracted coffee bean, which was also thermally treated originally, whereas sewage sludge is one of the most widely used waste materials and has the highest ratio of volatile matter to fixed carbon. However, the sludge also has the highest ash content among these particles, which is largely the cause of its low energy density and burnout time. The material analysis of these particles is shown in Table 1 and, the proximate and ultimate analyses are reported on an 'as received' and 'dry, ash-free' basis, respectively. These analysis data of four solid fuel particles were obtained from TGA-701 thermogravimeter, TruSpec elemental analyser and AC600 calorimeter at Energy & Environment Research Centre, KAIST. From the particle bulk density, the approximate energy density of subbituminous coal particles (19,581 MJ/m^3) is almost double that of the three biomass particles. Torrefied wood, coffee waste and sewage sludge particles have 11,890, 13,741 and 10,112 MJ/m^3 of energy density, respectively.

Figure 1. Pellets and single particles of the three biomass materials.

Table 1. Chemical compositions of biomass

Sample	Proximate analysis (wt. % ar)[1]				Ultimate analysis (wt. % daf)[2]					LHV[3&1] (MJ/kg)	Particle bulk density (g/cm^3)	Approx. energy density (MJ/m^3)
	V.M	F.C	Ash	M	C	H	O	N	S			
Torrefied wood	69.9	22.5	0.95	6.65	51.5	5.1	37.2	0.2	0	20.50	0.58	11,890
Coffee waste	72.9	11.1	5.8	10.2	49.4	5.7	35.3	2.6	0.4	20.82	0.66	13,741
Sewage sludge	61.2	7.89	25.0	5.91	38.6	5.9	20.6	0.9	0.1	17.14	0.59	10,112
Subbituminous coal (Adaro)	42.0	46.1	1.5	10.4	64.4	4.7	18.1	0.9	0.1	25.43	0.77	19,581

[1]as received [2]dry, ash free [3]lower heating value

Separation of biomass particles is approached cautiously because of their fibrous and tenacious nature, using several methods, including pulverisation (Step 1) and sieving (Step 2) processes shown in Fig. 2. Step 1 is a preliminary process to pulverise pellets into small particles. Step 2 separates the sample particles into 7 different sieve sizes: 150, 215, 250, 300, 355, 425 and 500 μm. An inclined plane (Step 3) is used to separate different shapes of

144 particles based on their translational and rotational motions. A1 uncoated paper on high-
145 density fibreboard was used for the shape separation process because matte and gloss coated
146 papers offered too low frictional resistance on the inclined planes. Sand paper could be a
147 potential option, but offered too much frictional resistance, holding dropped particles at the
148 top or midway down the inclined plane when this paper was used. The angle of the inclined
149 plane and drop distance of the particles were also significant parameters in this step. The
150 optimum angles were determined by a number of trials; a first plane has 45˚and second one,
151 60˚. Finally, high humidity and unclean surfaces must be avoided during the process.
152

153 In this experiment, irregular shapes, such as those which are extremely flat and cylindrical
154 with high aspect ratios, are not suitable for the cross-flow configuration. The undefined drag
155 coefficients obtained from these irregular shapes can lead to random trajectories with non-
156 uniform particle motion, resulting in non-quantitative analysis of burning particles. To reduce
157 this limitation, an inclined plane is used to separate particles based on their translational and
158 rotational motions, so as to collect particles of moderate shape, as shown in Fig. 2. Particles
159 with flat shapes stop at the upper zone of the first slope as they have the highest friction rate,
160 and cylindrical and spherical particles collect at the lower zone. The slope is then adjusted to
161 have different angles and the separation is run again on only the particles at the bottom, until
162 only spherical particles remain due to their lower inertial force. Using this approach, the
163 groups of spherical, cylindrical and flat shapes are prepared properly.

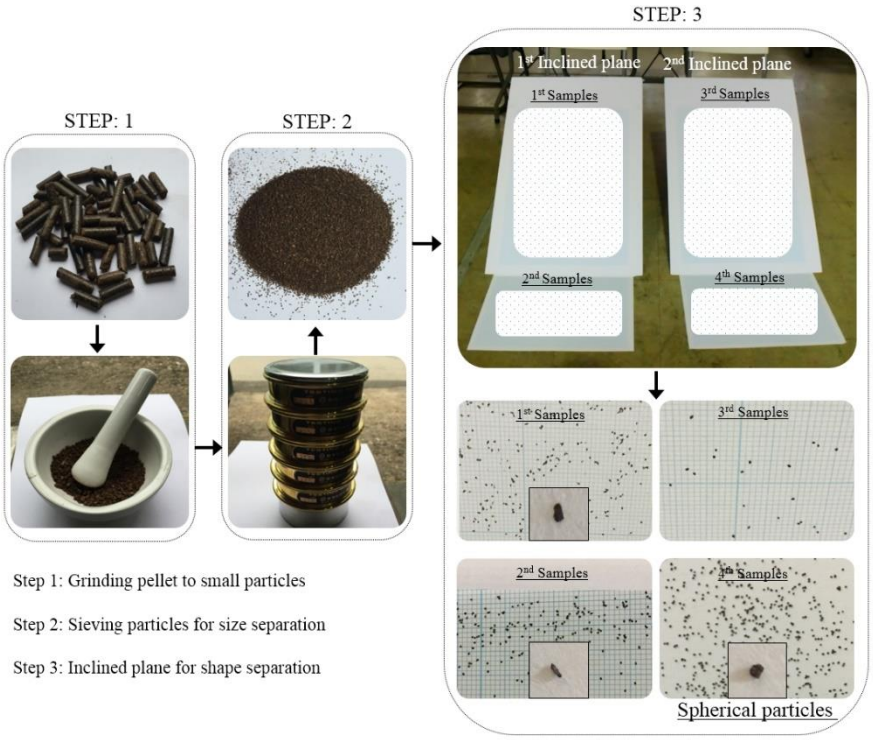

164

165 Figure 2. Pre-process for particle separation by means of sieving and inclined plane

166 methods.

167 *Single particle reactor coupled with cross-jet injection*

168 The laboratory-scale entrained single particle reactor shown in Fig. 3 has its gas

169 temperature, flow velocity and oxygen concentration controlled by the post-combustion gas,

170 guard heater and water-cooled injector. In this environment, a particle is expected to be

171 exposed to a uniform flow at high temperature to reduce experimental uncertainty from the

172 flow straightener. The reactor is made of a rectangular quartz cell of 45 mm × 45 mm × 500

173 mm to minimise the refractive index for observation of the combusting particle. The water-

174 cooled injector is installed to maintain the initial particle temperature of 298 K and the guard

175 heater forms the external wall of the cell to prevent large losses through heat transfer. The

176 single particle feeder is based on a fluidised bed of solid particles that are dropped from a

177 scientific syringe injector. Back pressure occurs in the double tubes, and the particles in the

fluidised bed are dropped into the particle injector. The measured number of particles inserted into a hot gas steam was 20-30 particles/min. The flow rate of the carrier gas in the particle injector is determined to be 0.5 L/min to lift particles over 150 μm. The upward and vertical flow velocities are constant for all particles, to investigate comparable combustion time and particle displacement.

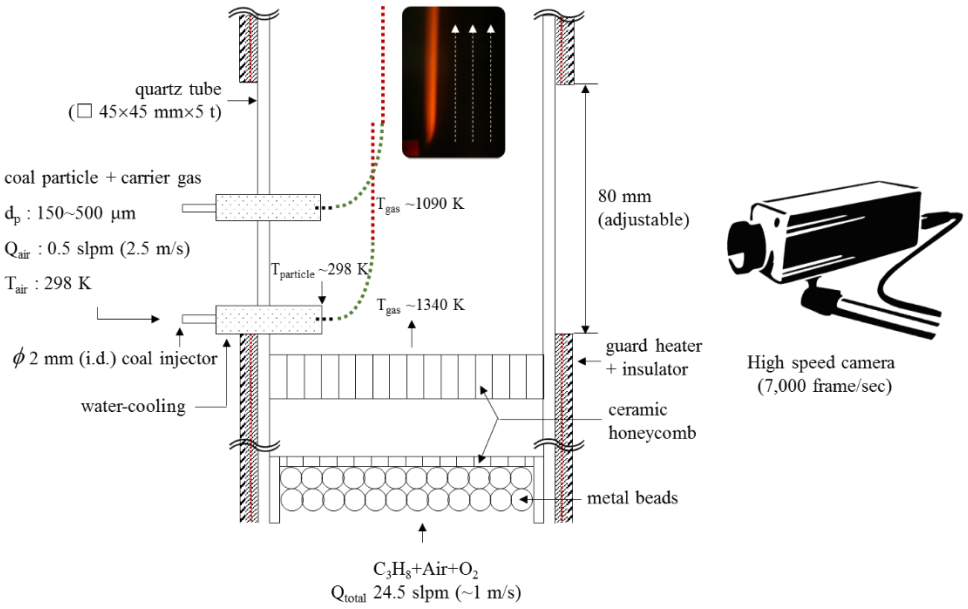

Figure 3. Schematic diagram of the experimental setup at 1,090 K and 1,340 K of gas temperatures.

Operating conditions and particle size

The post-combustion gas produces a high temperature in the upward stream from the honeycomb. In the quartz cell, substantial heat loss is inevitable between the wall and a hot gas stream, in which a high temperature gradient appears and particles pass through. The environment gas temperature is calculated on the basis of the radiation loss of the probe of an R-type thermocouple [23]. The temperature profile is shown in Fig. 4. The high-mixing zone between the leftward-flowing cold carrier gas and the upward-flowing hot gas stream is

clearly shown to affect transient combustion behaviour. Particle temperature before injection remains at 298 K and reaches a certain high temperature as a particle passes through the hot gas stream. To avoid large heat loss, the position of the injector is located 10 mm from the wall.

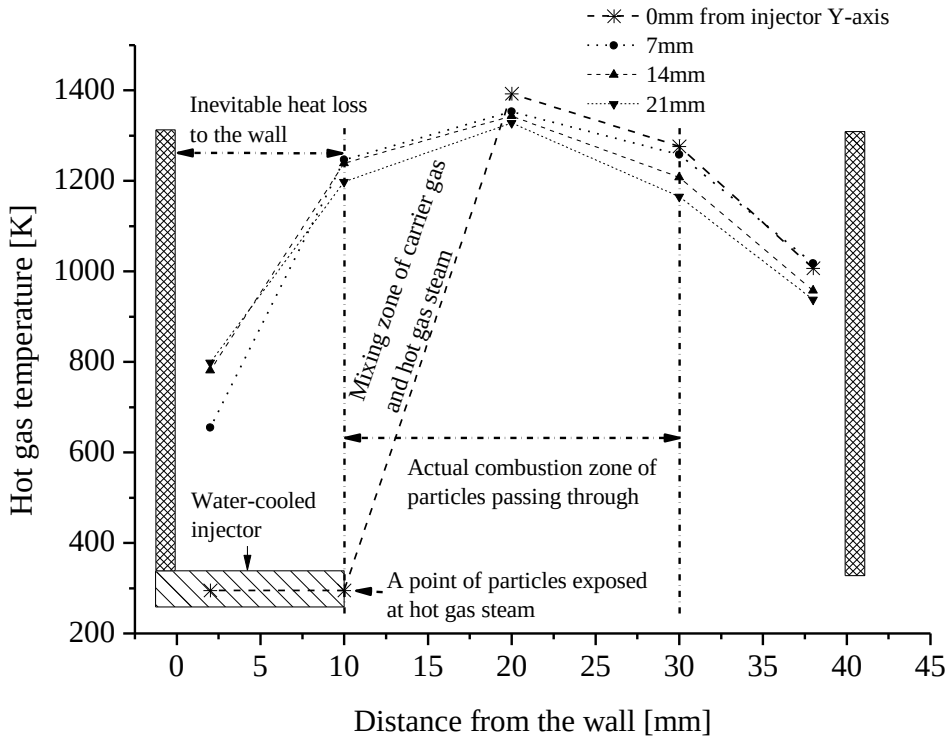

Figure 4. Temperature profiles measured from the experiment.

The amount of oxygen is supplemented from 10.4 % to 40.1 % of the total product gases. After the combustion of C_3H_8, flue gases such as N_2 (38.2–67.9 %), O_2 (10.4–40.1 %), H_2O (12.4 %) and CO_2 (9.3 %) are yielded. The group sizes of the solid particles are prepared in nominal size ranges of 150–215, 255–300, 355–400 and 400–500 μm to determine the largest size at which the particles are burned completely.

Observation of the biomass particles

A high-speed camera (Phantom V710) is used to observe burning particles at 5,000–7,000

frames per second with a micro-lens and back lighting. It is equipped with a complementary metal oxide semiconductor (CMOS) image sensor of size 25.6 mm × 16.0 mm with a resolution of 1,280 × 800 pixels, and is capable of recording the motions of particles. This camera enables analysis of the combustion of a single particle in great detail. The observation zone is extended by adjusting the micro-lens, as the prepared biomass particles are larger than those in previous experiments [24, 25], and the calibration is carried out with a circle-scale reticle. The size of a pixel is measured to be 58 μm and, a light-emitting diode (LED) backlight at 5,600 K (colour temperature) is installed at the rear of the quartz cell. This enables direct observation of a burning particle's ignition, flame structure and char combustion.

Mechanism of biomass pyrolysis and sequential combustion regimes

Biomass contains a variety of proportions of cellulose, hemicellulose and lignin, which results in variations in the gas-eruption profile and mass reduction that depend on the type of biomass [26]. It is widely accepted that hemicellulose is decomposed at a temperature range of 493–588 K, cellulose at 588–673 K and lignin over a wide range of 433–1,173 K [27]. The typical gases produced by biomass combustion include H_2, CO, CO_2, H_2O and CH_4 as light hydrocarbons, as well as tar and char in primary pyrolysis. It is generally assumed that char combustion starts successively after the volatile flame is dissipated as volatiles evolution is fast enough to move the pyrolysis zone away from the particle surface [28, 29]. This is referred to as a sequential combustion process and, a typical sequential process of a particle in the experiment is shown in Fig. 5. Char combustion may occur in early gas-phase combustion stage, if oxygen reaches the particle surface. This burning behaviour is called a simultaneous combustion process [30, 31]. In simultaneous combustion, the volatile flame

does not lift off the surface and the flame possesses a thin structure. Overlapping combustion is attributed to low gas temperature, small particles and the specific type of particle [32]. In addition, the irregular shapes of the biomass particle and the volatility of the flame may contribute to overlapping combustion. Consequently, the physical characteristics of the volatile flame on biomass particles in the early combustion stage have a significant role in determining the combustion process.

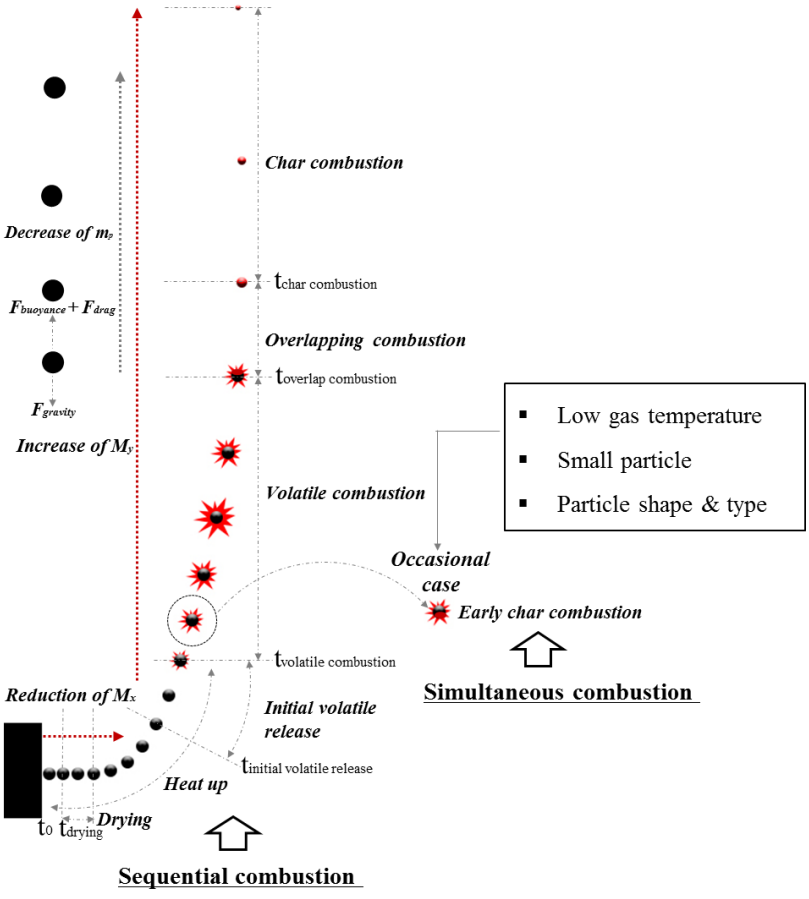

Figure 5. Sequential regimes of a solid fuel particle during combustion.

Results and Discussion

SEM images observed from biomass particles

The scanning electron microscope (SEM) images of the three raw biomass types during the combustion process are shown in Fig. 6. These particles were collected from the electric furnace where the hot gas temperature is identical to that in the entrained flow reactor. The burning particle after volatile ignition with the maximum size of flame was ejected from the furnace and then quenched quickly on a cold plate. For the particle image of char combustion, the particle was prepared after extinction of its flame. The NOVA 230 SEM was employed at KAIST and, the backscattered images were captured under the following parameters: Acc.V: 10.0 kV, Spot: 3.0 and Magn: 650-800 x. The external physical structures, with their small pores and irregular shapes, are remarkably similar between raw torrefied wood and coffee waste. However, torrefied wood contains a high proportion of fibrous cellulose in its transformed structures due to thermal pre-treatment. Raw coffee waste is a physically mixed formation with a number of small cumulative particles along with porosity. Raw sewage sludge closely resembles a stiff clay soil with less porous surfaces. During combustion processes, these raw biomass particles experience an increase in porous surface with a certain swelling due to the melting and softening of the particles. Torrefied wood shows a significant physical transformation at high environmental temperature during the combustion process. Compared with coffee waste and torrefied wood, sewage sludge has numerous cracks on its surface. The particles of all chars are apparently deformed from the shapes of the raw particles due to release of volatile matter and subsequent physical deformation, and the particle volume starts to decrease due to surface oxidation.

Figure 6. SEM images of three different biomass types. In the upper row, raw particles of torrefied wood, coffee waste and sewage sludge are shown and the time series of the physical deformation of these three particles during combustion are presented along each column.

Observation of the sequential combustion process and its characteristic flame structure

For an explicit description of sequential combustion processes, a particle injected from the tip of the water-cooled injector is maintained at 298 K and the combustion is assumed to begin (t = 0) when it is exposed to a hot gas stream. The particle is first heated up with the initial drying process and then starts to release volatile matter, upon which it is immediately ignited after gas erupts from the solid particle. After these stages, a flame is observed away from the surface of the particle, forming a luminous boundary at which oxidation of the product gas takes place through a secondary particle reaction. The degree of luminosity is dominantly attributed to soot density in the flame and can be increased by using a hotter gas stream or particle temperature. The entire development of a volatile flame from the ignition of the gas

phase to its extinction is observed to take place for particle size of 150–215 μm at all oxygen concentrations. Complete observation of the period for particle size 425–500 μm is limited due to limitation of the visualisation field. Photographic images of three particles are superimposed over a time interval of 2 ms in Fig. 7. This enables a distinct description of a burning particle as it is displaced along with the development of its volatile flame structure. These results help to predict the mass reduction of particles because of the cross-flow configuration. In this layout, a particle starts drying very quickly in the mixing zone of the horizontal and vertical streams, and then moves in the horizontal direction at high momentum due to the cold carrier gas. After passing through the transient point, rotating particles go upward because of the buoyancy and drag force acting on the particle overcoming gravity.

For sequential combustions at 21 % O_2 and 150–215 μm particle size, different combustion behaviour in terms of residence time and displacement is seen for the four particle types. A coal particle undergoes a sequential combustion process; this particle has a flame with high soot content and experiences a shorter period of volatile combustion than do the three biomass particles because of the presence of less volatile matter. The charred coal immediately experiences oxidation after extinction of the homogenous combustion. On the other hand, torrefied wood and coffee waste have volatile flames with different physical structures from that of the coal particle. The relatively sooty flame for torrefied wood lasts 30 ms, whereas coffee waste has a very thin flame with duration of volatile combustion of approximately 14 ms. The different durations can be attributed to interactions between volatile matter content and soot formation. An increase in particle temperature leads to a change in its structure because of a high mass-reduction rate. During the combustion process, temperatures of the particle and the flame are much different. Timothy et al. [33] reported that the surface temperature while the flame envelope exists is even lower than the temperature of

the flame. Finally, sewage sludge initially has an unclear volatile flame, which then forms a thin, nearly transparent volatile flame at an early stage due to its low carbon content.

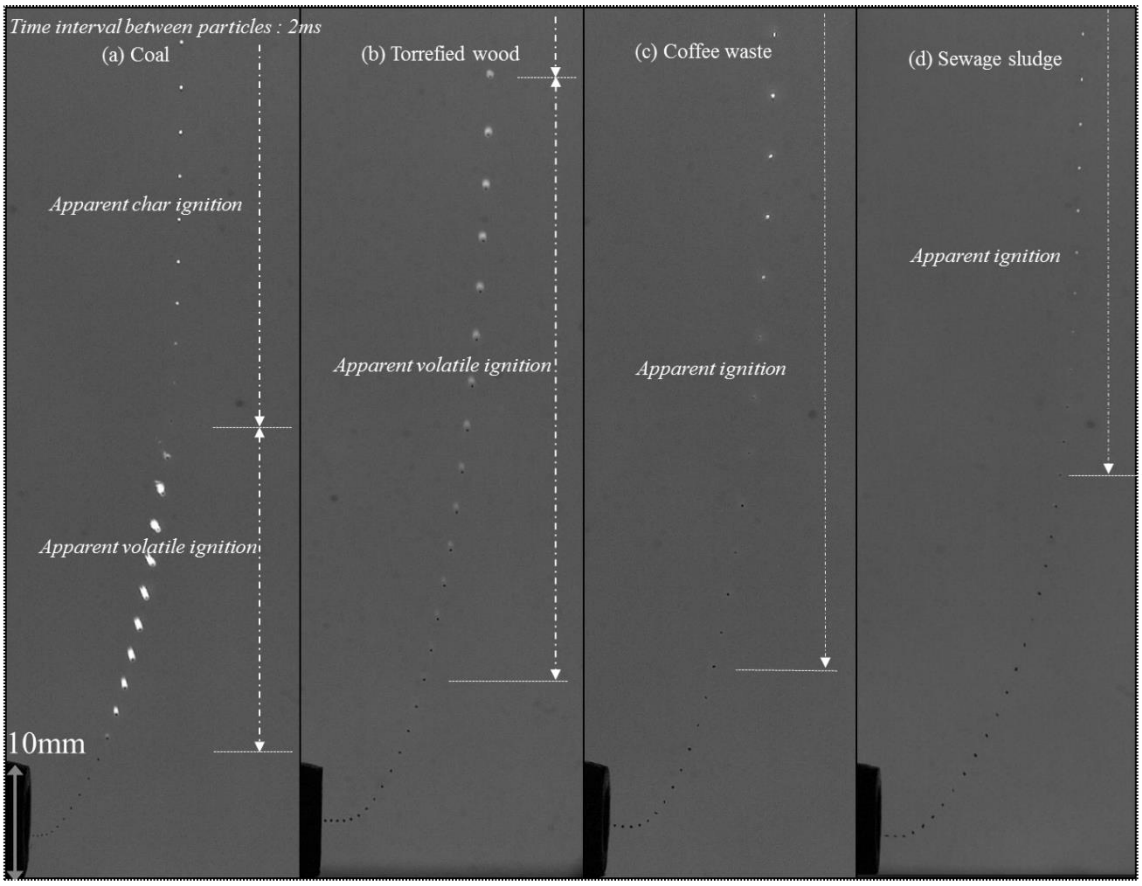

Figure 7. Sequential combustion process including overlapping and char combustion for 155–215 μm particles of four different samples at 21 % oxygen concentration and 1340 K: (a) sub-bituminous coal, (b) torrefied wood, (c) coffee waste, and (d) sewage sludge.

To provide a comparative analysis of sooty flames for particles with different physical structures, the superimposed images of four solid particles at 300–355 μm and 10 % O_2 are captured at identical conditions shown in Fig. 8. In general, biomass has an early initial release of volatile matter compared with coal at a low heating rate, such as in a thermogravimetric analyser. Sub-bituminous coal ignites a bit earlier compared with the three biomass particles in the same particle size group. Different onset times of ignition between

biomass particles are also observed and can be attributed to their compositions and physical structures.

The flames of burning biomass particles are relatively smaller and less sooty than those of coal due to the relative soot formations from reactions with tar at high temperature. It is accepted that this physical configuration is dominantly determined by complicated interactions between volatile matter, carbon content, particle density and different rates of devolatilisation. The three biomass particles have less bulk density, compared to the coal particle density (0.77g/cm^3); the densities of torrefied wood, coffee waste and sewage sludge are 0.72, 0.86 and 0.76 times that of coal, respectively. This low density of biomass particles may result a shorter gas-phase combustion. However, these biomass particles have higher mass volume fraction of volatile matter to coal, and thus, the duration of gas-phase combustion for biomass is still longer than that of coal; from bulk density measurements, torrefied wood, coffee waste and sewage sludge have 1.9, 2.3 and 1.7 g in equal volumes, while coal still has the lowest mass of volatile content at 1.6 g although it has a higher bulk density. The calculation measured total mass of torrefied wood (2.71 g), coffee waste (3.20 g) and sewage sludge (2.84 g) in 4.82 cm^3 and the mass fraction of volatile matter of each particle type is given in Table 1. In addition, the mass of fixed carbon of torrefied wood, coffee waste and sewage sludge is 0.6, 0.4 and 0.2 g, respectively, while coal has 1.7 g; this leads to the differing char combustion behaviour between biomass and coal particles. That is, volatile matter content is a major factor in determining combustion time. Under direct observation, an elongated flame is detected on all particles at 10 % oxygen concentration. The shape of the flame structures is due to the low diffusion rate of oxygen with the effect of buoyancy and it is apparent that coal has the flame with the highest aspect ratio. At this particle size group, biomass particles have even higher elongated flames than that at 150–215

μm because a larger volume particle contains more volatile matter and carbon content.

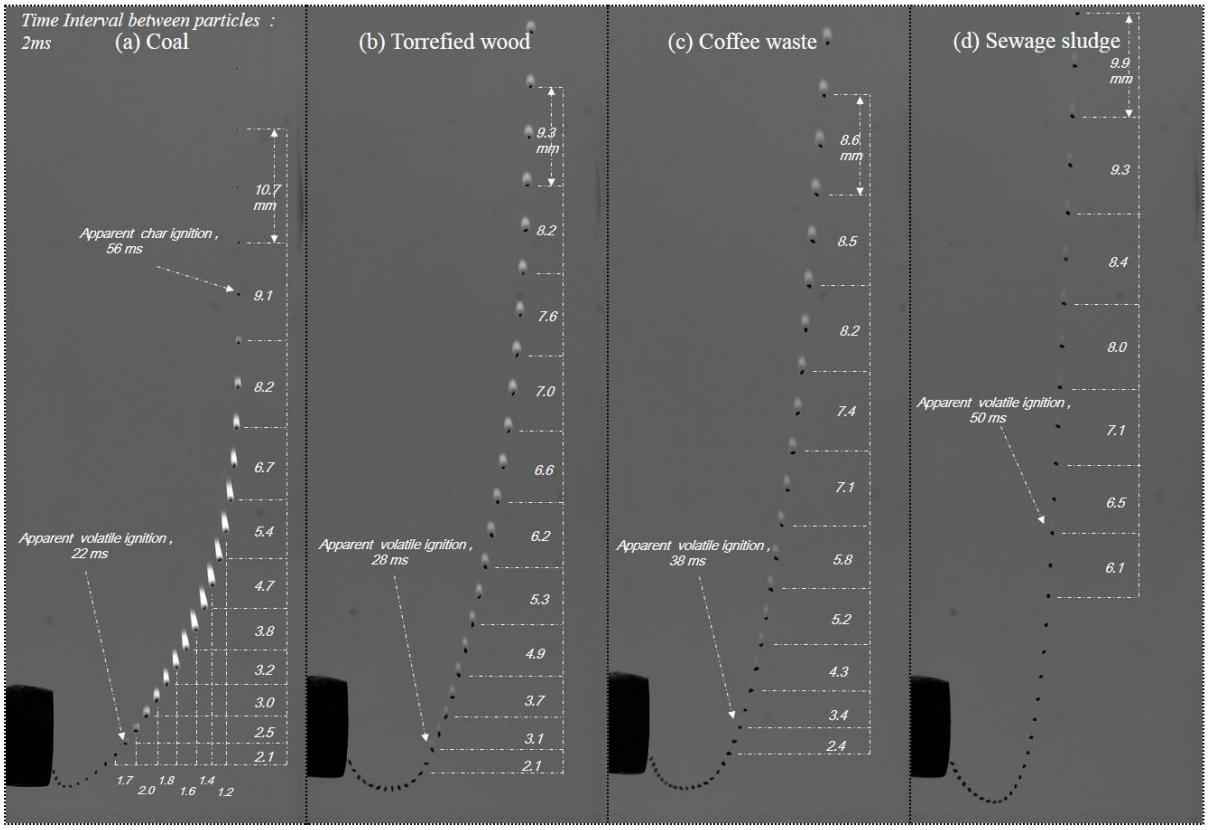

Figure 8. Flame structures and luminosities of the superimposed coal and biomass particles entrained into hot gas streams of 1,340 K (300–355 μm, 10 % oxygen concentration). The particle displacement after the injection is marked in the time interval of 2 ms and apparent volatile ignition occurs within a few milliseconds depending on the type of solid particle.

The intensity of volatile flames for the four particles is converted into a greyscale image by means of a numerical data matrix shown in Fig. 9. Identical backlighting is used in all images to minimise the error in the numerical solution. In the imaging process, each pixel of the image presents light intensity on a greyscale from 0 to 255, and the numerical backlighting data are extracted from the images. The intensity of the flame is then divided by the maximum value of grayscale (255) for comparative analysis of each image. Coal has max.

43.2 % of the highest intensity between 0.78 and 1 in the luminous flam whereas torrefied wood, coffee waste and sewage sludge account for 13.4, 10.4 and 4.1 %, respectively.

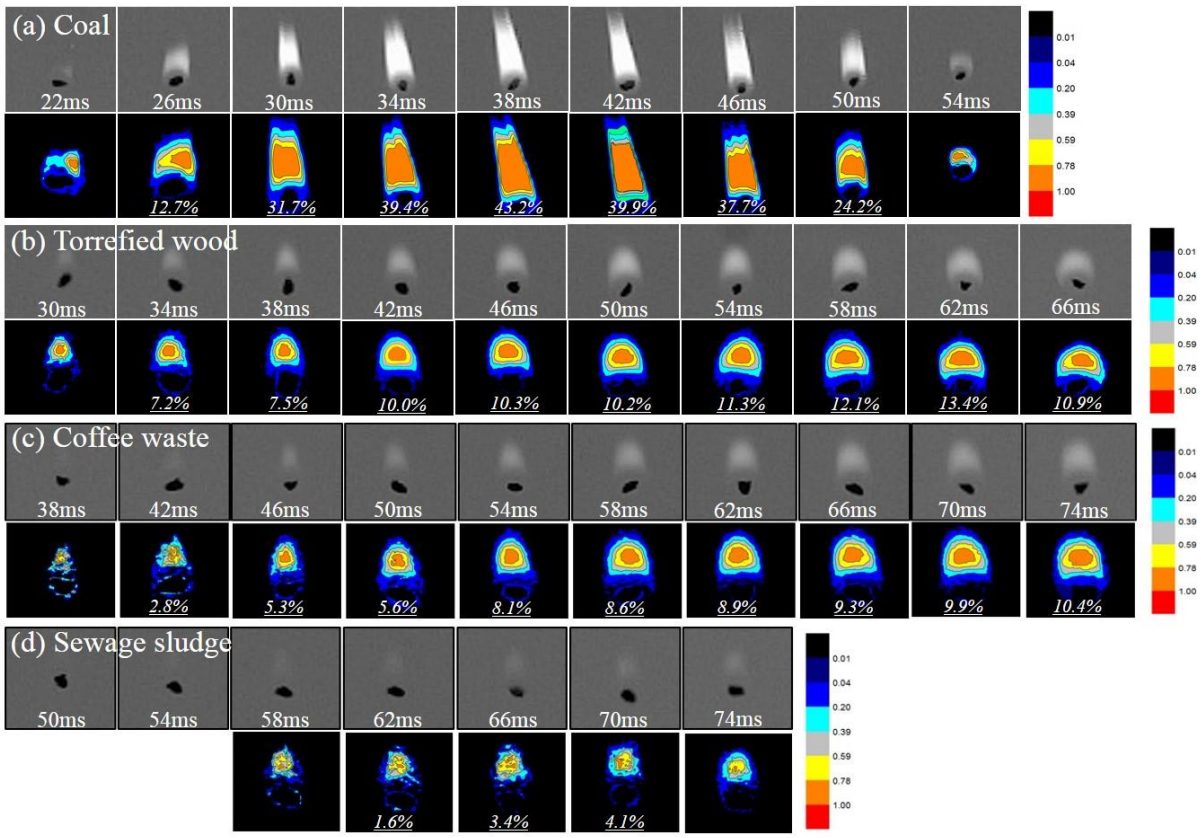

Figure 9. Captured images obtained from burning particles of 300–355 μm and the normalised intensity of their flames represented by the imaging process.

Effects of biomass type and enhanced O_2 concentration

The comparative combustion behaviour for different biomass types and different O_2 concentrations are presented in a series of images shown in Fig. 10. Increase in the oxygen concentration for each particle is revealed to result in different physical structures of the volatile flames with different onset times of ignition. The earlier apparent ignition of coal occurs at all oxygen concentrations, and the biomass flame size is smaller than that of coal for all size groups examined. However, the three biomass types had different flame intensities

with different ignition delays and overlapping combustion at the early stage. Torrefied wood, coffee waste and sewage sludge manifest different changes with oxygen concentration. Kuo et al. [34] pointed out that ignition behaviour such as the structures of the volatile flame, ignition time and early ignition are mainly determined by the properties of the biomass. Normalised intensities of actual flames for different particles are shown in Fig. 11, but a whole period is not detected until the extinction of volatile flame because of the limitation of the visualisation section. The size of volatile flame on a particle exhibits a nearly symmetrical profile, as indicated by the experimental results. Therefore, the unmeasured data due to the limited visualisation field were predicted in Fig 11 and 12. Fig. 11 presents the profiles with predicted values. Based on a previous study [35], these differences between particles are partly attributed to different ratios of hydrogen to carbon, which affect the soot volume fraction. The particle is heated by radiation from the soot flame by a feedback mechanism [29] along with the combustion front and also by convection from a hot gas stream in the reactor. For that reason, the particle temperature is affected by the degree of soot flame. Accordingly, low soot and invisible flames influence ignition delay, flame instability and low radiation in the visible and near-infrared spectral ranges. The radiation from emission of soot particles in a flame has an important role in burning and spread rates [36–39].

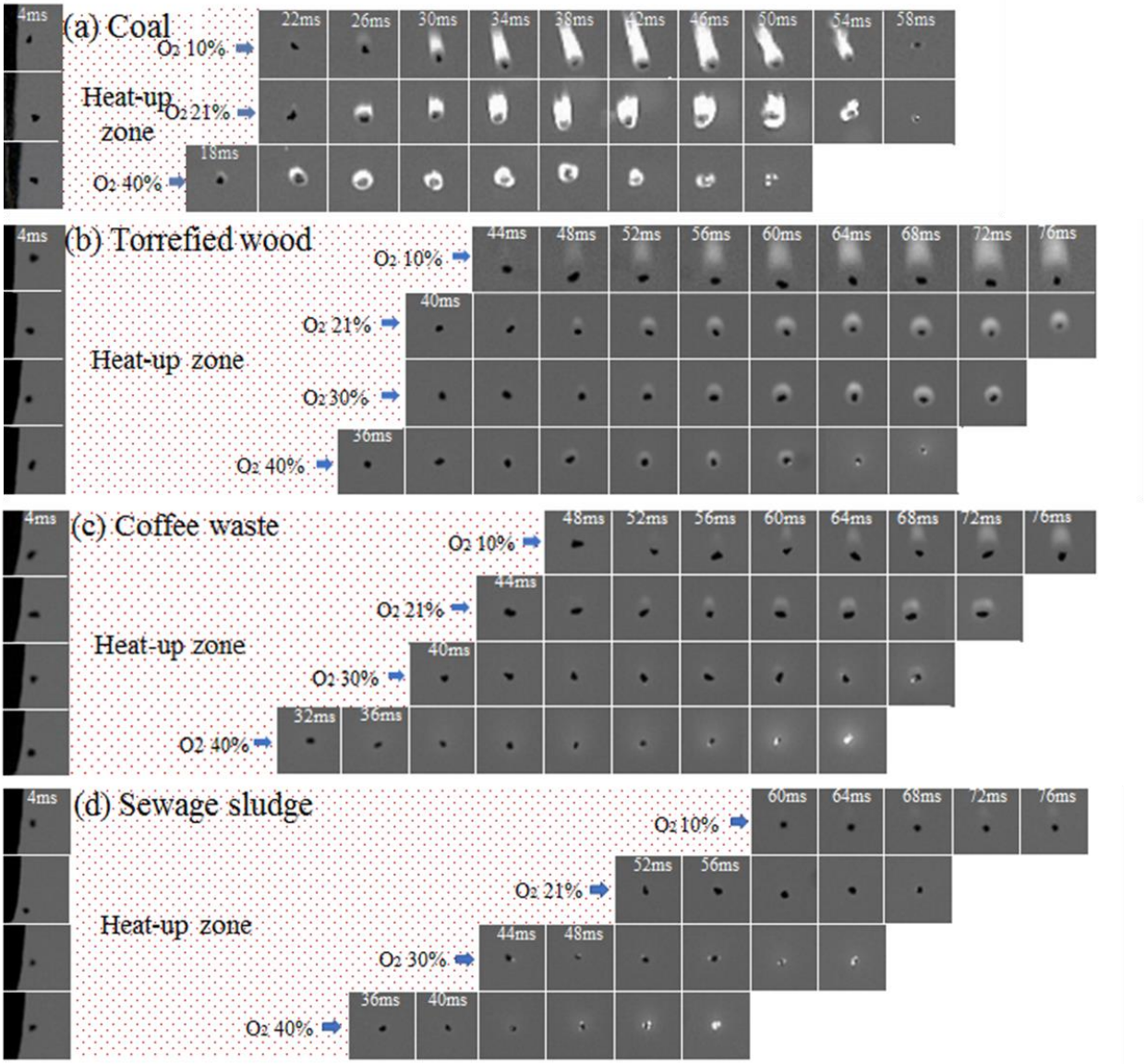

Figure 10. Comparative combustion behaviour over time intervals of 4 ms, obtained from the set of burning particles of size 255–300 μm at 1340 K as the oxygen concentration is increased.

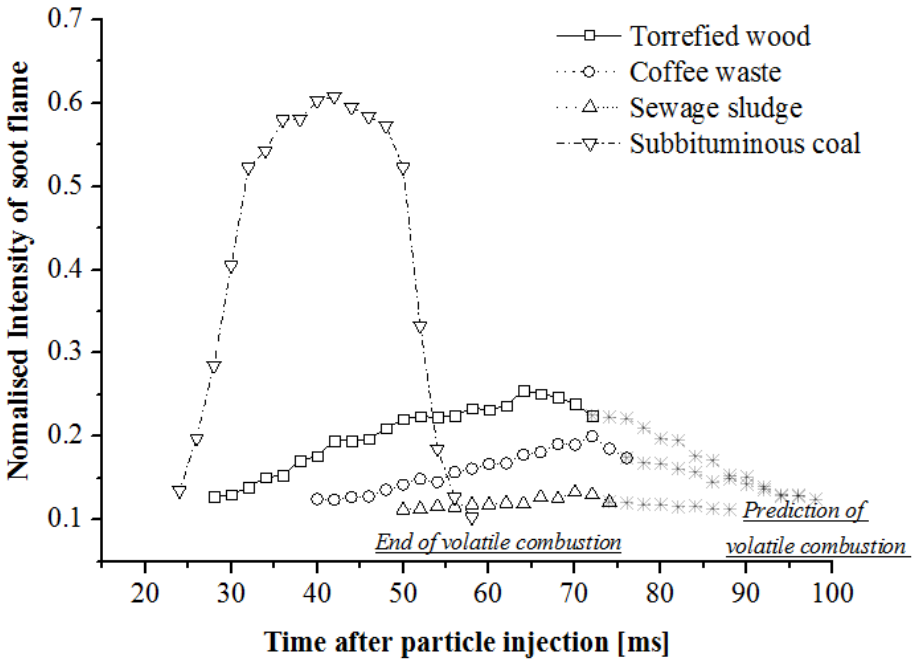

Figure 11. Effect of different fuel particles measured from grayscale images of 300–355 μm particles exposed at 1340 K. Biomass particles are still burning during the volatile combustion stages and the predicted lines of the volatile flame are extended due to the symmetrical tendency of the patterns.

The ratio of the radii of effective flame to particle size is plotted for the biomass particles as a function of the oxygen concentration, as shown in Fig. 12. The profile which has unmeasured flame is also extended to predict the whole flame history. The effective maximum ratio between torrefied wood, coffee waste and sewage sludge with 255–300 μm particles varies by 5.2, 3.5 and 3.4, respectively, at 10% oxygen concentration. The size of the volatile cloud decreases with a shorter duration of devolatilisation as the oxygen concentration increases. Previous work [24, 40] reported that a fast mass reduction during devolatilisation is due to higher oxidation of the gas phase. The decreases in the radius and shorter duration are only clearly observed in torrefied wood and coffee waste over all enhanced oxygen concentrations.

The radius for sewage sludge is not detected when the oxygen concentration is over 21 % as the particle has too little soot and an invisibly thin flame. Interestingly, the reduction in volatile radius is remarkable in torrefied wood as oxygen concentration varies between 10 % and 20 %. It is believed that sewage sludge particles below 255–300 μm have significantly low radiant energy due to thin and invisible flames, which may affect power generation in a pulverised biomass plant. These flame structures, which contain soot particles and gas phase, have an important role in radiant energy. The energy is attributed to the flame size and its high intensity and, the measured parametric values can be discussed by time-averaged radiation [41], $Qr=\sigma\varepsilon_T T_f^4 A_f$ where σ is the Stefan-Boltzmann constant (5.67×10^{-11} kW/m^{2}K^4), ε_T is the flame emissivity, T_f^4 is the average flame radiation temperature and A_f is the flame surface area.

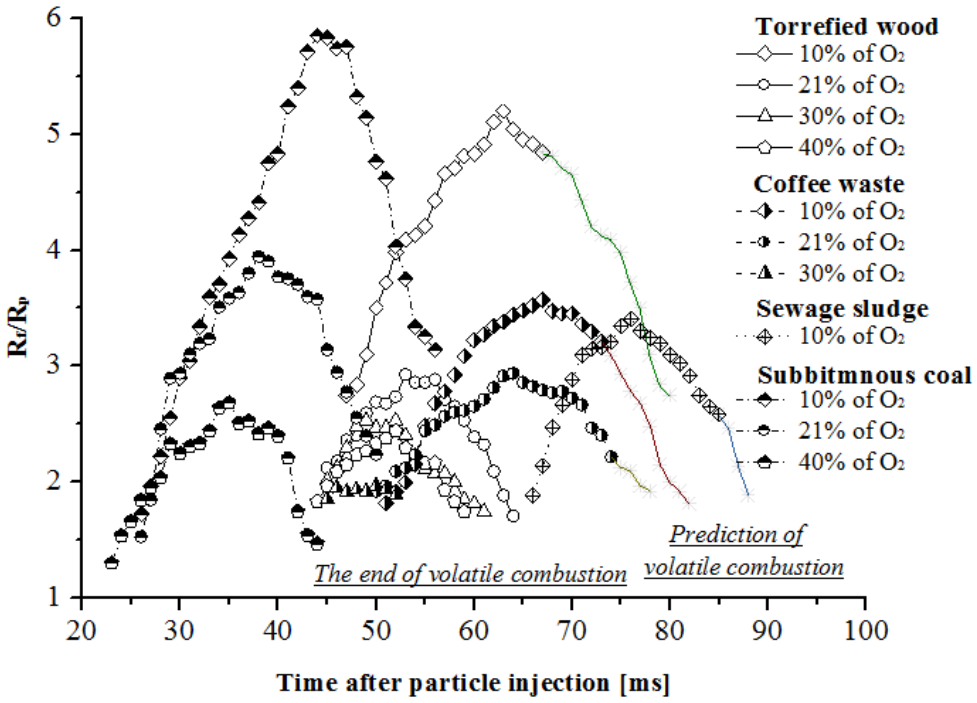

Figure 12. Effect of oxygen concentration on torrefied wood, coffee waste and sewage sludge with 255–300 μm particles at 1340 K. Volatile flames of sewage sludge are not detected for

oxygen concentrations over 21 % due to low soot and very thin volatile cloud formation.

Average ignition delay against time is analysed for the three biomass particle types of 155–215 μm and all oxygen concentrations, as shown in Fig. 13. It is apparent that the heating time and durations of homogenous and heterogeneous combustion decrease as oxygen diffusivity increases. From the figure, longer volatile combustion and shorter overlapping combustion are observed in torrefied wood (which has experienced thermal pre-treatment), whereas coffee waste and sewage sludge have relatively shorter durations of volatile combustion. In the case of 155–215 μm particles, early onset of char ignition appears only for coffee waste and sewage sludge, which may be related to the rapid increase in particle temperature, enabling a shorter duration of devolatilisation.

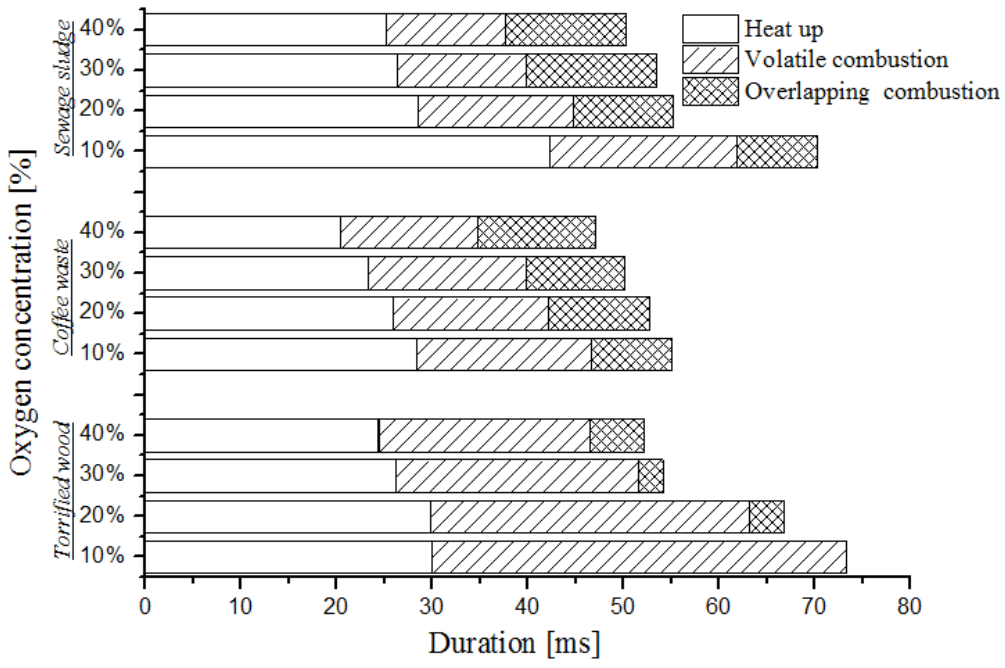

Figure 13. Average duration of heat up and the end of volatile combustion for three biomass particles (155–215 μm) at 1340 K, and quantitative measurements of burning time vs. oxygen concentrations.

Effect of environmental gas temperature on combustion behaviour

The burning of particles enable discussion of the effect of temperature conditions on combustion behaviour. At 1090 K and 1340 K, the trajectories of coal and torrefied wood are compared in Fig. 14 to characterise the volatile flames. Both particles at 1090 K form volatile flames of smaller sizes with lower intensity, and the flame of torrefied biomass even becomes transparent with longer ignition delay. This suggests that significant soot formation does not occur at low temperature, along with low volatile release rate, as compared with a higher gas temperature of 1340 K. Fig. 15 shows that the average duration of heat-up at 1090 K is longer than that at 1340 K. The apparent change in the heat-up duration at low temperature as a function of oxygen concentration is more prominent than that at 1340 K. This is consistent with the result from a previous study [6], which showed that the effect of oxygen concentration on ignition delay and burnout time is expected to be slightly more pronounced at lower temperature.

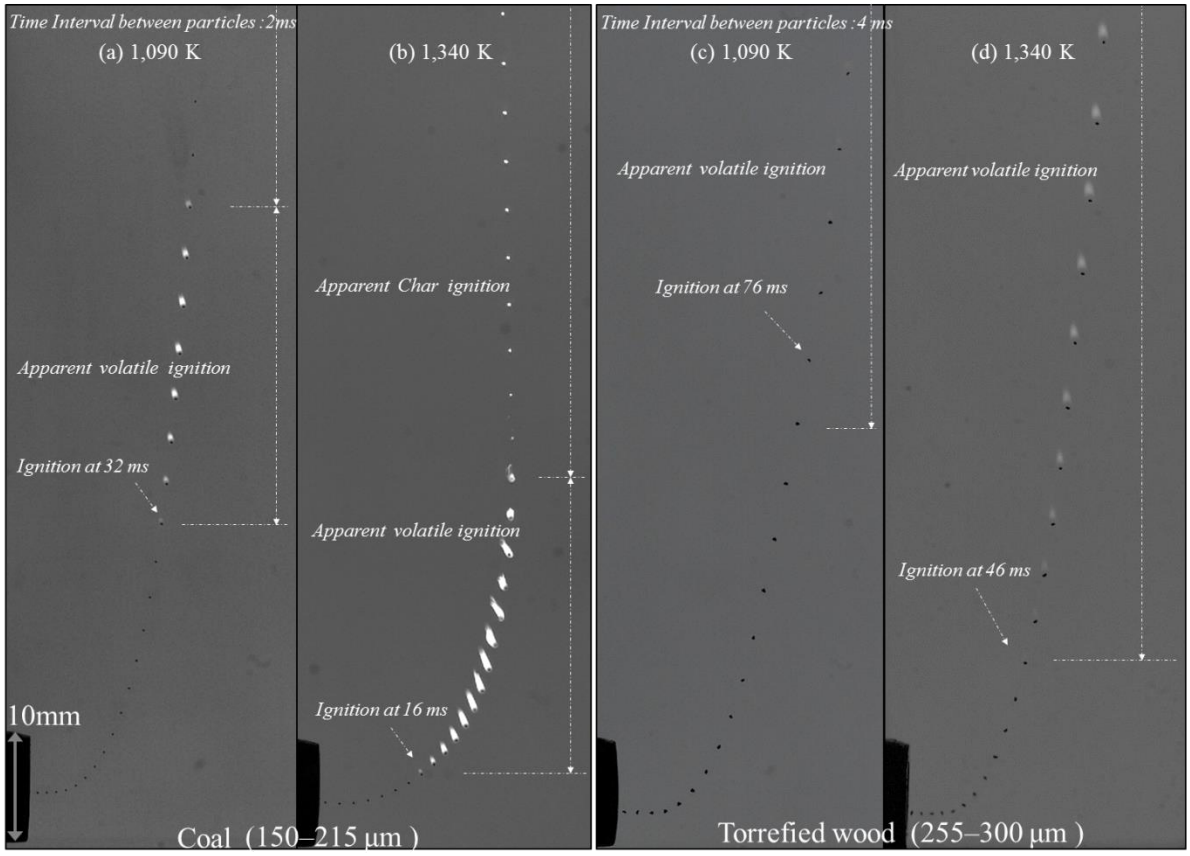

443

444 Figure 14. Comparative volatile flames and ignition behaviour of coal and torrefied wood
445 between 1090 K and 1340 K at 10% of O_2: coal, 150–215 µm and torrefied wood, 255–300
446 µm.

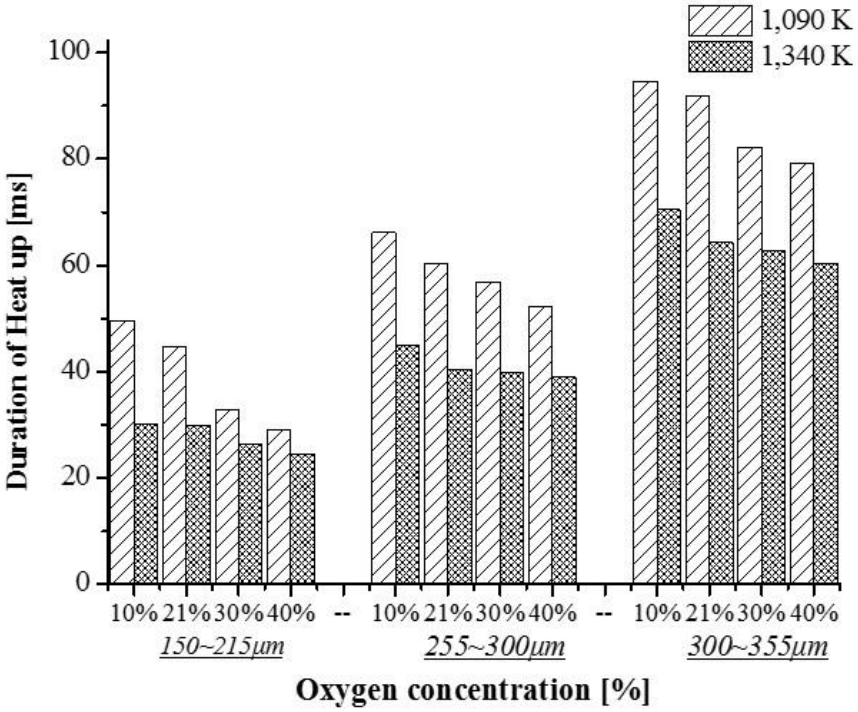

Figure 15. Average duration of heat up for torrefied wood particles of 150–355 μm under different gas temperature and oxygen concentration conditions.

Effect of particle size on combustion behaviour

Several researchers [42, 43] have studied intra-particle effects during combustion. In general, the temperature of a large-sized particle is controlled by the surrounding temperature and this particle has an intra-particle temperature gradient. However, a pulverised particle under 200 μm has a small temperature gradient which does not affect the rate of devolatilisation [15, 44]. Fig. 16 illustrates the average duration of heat-up for particles of each of the three biomass types with particle size in the range from 150–215 μm to 355x425 μm, each taken over 20 particle samples. The transience point of ignition delay for torrified wood occurs at the size group of 255–300 μm and coffee waste at 215–255 μm, where average time of heat-up increases more sharply, probably due to an intra-particle effect.

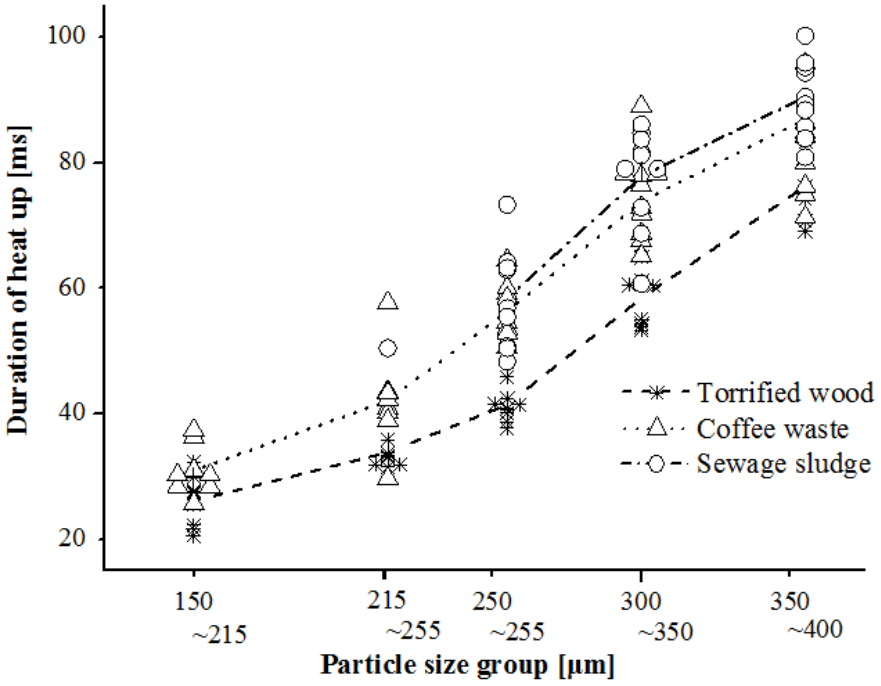

460

461 Figure 16. Experimental data on ignition delay for biomass particles in the range 150–400
462 µm at 1340 K and 21 % oxygen concentration.

463 Fig. 17 illustrates the maximum effective radius of volatile flame for particles in the ranges
464 from 155–215 µm to 355–425 µm under oxygen concentrations of 10 and 21 %. First, a
465 higher effective radius is quantitatively measured at low oxygen concentration for all
466 particles. Second, R_f/R_p in torrefied wood undergoes only a marginal change with a relatively
467 sooty flame from 155–215 µm to 355–425 µm at 10 % oxygen concentration. However, this
468 radius (R_f/R_p) decreases with particle size increase at 21 % oxygen concentration. The radius
469 of torrefied wood and coffee waste with 255–300 µm particles is almost equal to that at 21%
470 oxygen concentration, but coffee waste has a very thin, low soot flame when its particle size
471 is 155–215 µm. Consequently, coffee waste is required to be at least 255–300 µm in size to
472 achieve an equivalent flame structure to torrefied wood. Finally, an invisible or very thin
473 flame is detected for sewage sludge when it is burned at 21 % oxygen concentration. The raw
474 sewage sludge in these experimental conditions is low combustion quality of biomass. An

increase in sludge particle size might enhance the flame stability, but a large particle would drop to the bottom of the reactor without combustion. To avoid this, a higher gas temperature or thermal pre-treatment of sewage sludge might be required.

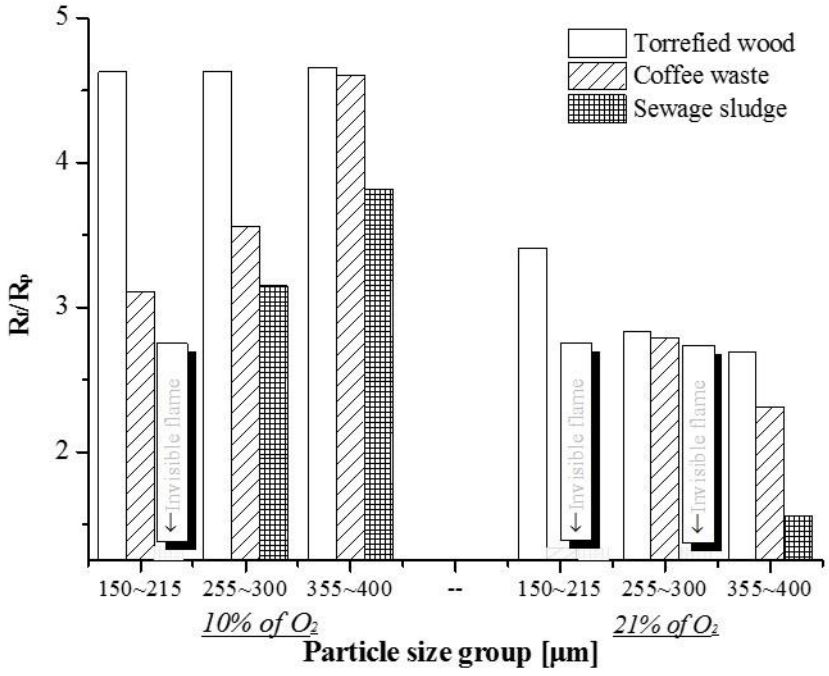

Figure 17. Average effective flame radii of three biomass particle types in the range 150–400 μm between 10 % and 20 % oxygen concentration.

Discussion of special cases

Ignition behaviour and flame instability

Ignition behaviour is determined by interactions between complicated factors such as the physical and chemical characteristics of the biomass and the surrounding environment as well as operating conditions. Variation in the composition could enable a longer ignition delay, smaller soot cloud and earlier fragmentation with the instability of the volatile flame. The investigation of ignition delay as a function of certain parameters may provide partial

answers concerning optimised particle combustion. Fig. 18 shows the onset time of volatile ignition, earlier overlapping combustion and the visible structure of volatile flame in different environmental conditions. There are four observations of burning particles in different environmental conditions. The two different gas temperatures were used to simulate the moisture and oxy-fuel combustion effects. For high mass volume of moisture, particles were put in a closed container (20 cm×20 cm) on a hot plate at 323 K. There was a sponge with high moisture in the bottom of the container, with no particle-sponge contact. The group of particles was kept in the container for 4 hours at 95 % absolute humidity. As a consequence, 25 % moisture was added to the particles. The particles which were out of the container had to be tested quickly because this moisture content was likely to be evaporated in a short time. To compare O_2/N_2 and O_2/CO_2 environments, CO_2 for 21% O_2 concentration was supplied from the post combustion burner, instead of air. First, the flame instability is found to be related to environmental temperature. A previous study [34] observed a different model of ignition obtained from anisotropy of the thermal properties of large biomass particles and reported that different ignition behaviour was determined by the surrounding gas temperature. Second, moisture content enhanced the ignition delay at the early stage, which caused earlier char combustion with the formation of a thin flame. Kucuk et al. [45] pointed out that the evaporation of moisture leads to an increase in char combustion to be attacked by oxygen due to the formation of an active centre. Lastly, early ignition and flame instability of a particle occur under CO_2 atmosphere due to the high thermal capacity of CO_2 and the high reactivity of char-CO_2, as reported by Shaddix et al. [22].

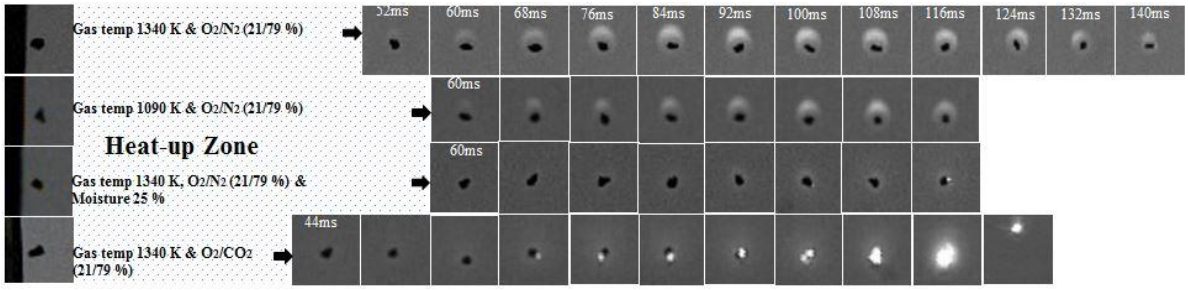

Figure 18. Comparison of combustion behaviour on coffee waste particles for four different environmental conditions.

Insights into flame formation are essential to understand combustion behaviour, such as flame stability, to better determine the operating conditions and select appropriate biomass. Fig. 19 illustrates two types of volatile flames that are observed for a single particle and a pellet of coffee waste. As mentioned before, coffee and sludge particles typically have a thinner volatile flame or an invisible flame compared with torrefied wood particles. At high oxygen concentrations, scattered volatile gases and small particles that escape from parent particles are detected above an invisible or very thin diffusion flame. From the observation, the actual size of the flame can be reduced during the combustion process. To support this flame instability, a pelletised biomass particle is examined at the same gas temperature. The size of diffusion flame at 40 % of O_2 is apparently smaller than that at 20 % of O_2, and this flame partially detached over an enlarged scattering flame at high oxygen concentration. This phenomenon is attributed to rapid escape of high-volatility matter and particles from a luminous flame without any reaction. Consequently, the onset of volatile scattering enables the formation of very thin volatile flames with relatively low soot content. These results are consistent with the work of Holtmeyer et al. [46], who studied combustion modes through experimental and numerical methods. The mechanism of this volatile scattering is not clearly defined, but it is frequently experienced by biomass with highly volatile content, anisotropic release and a low-soot flame above a diffusion flame.

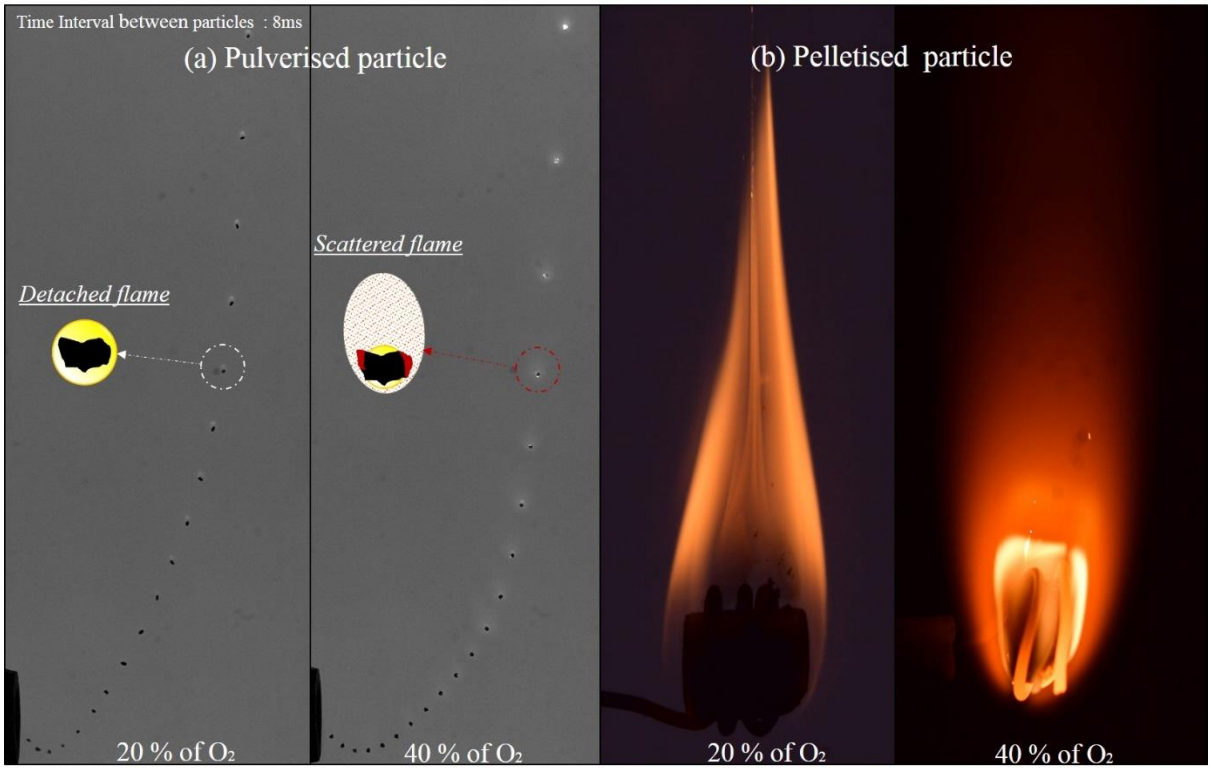

Figure 19. Different modes of the volatile flame of coffee waste produced under enhanced oxygen concentration.

Overlapping combustion at an early stage and fragmentation

Overlapping combustion is attributed to low gas temperature, rapid heating rate, small particles and low flame formation. In addition, the shapes of the particle, the different rotational speeds between them and the volatility of the flame may be related to the overlapping combustion shown in Fig. 20. Normally, the volatile flame with an O_2 concentration over 21 % has a relatively thin spherical shape for an irregular particle. From the figure, we note that the particle exposed to a hot gas stream starts rotational motion, and then a volatile flame is formed after volatile matter release. In the process, the different rotational speeds of the particle and volatile flame are detected after volatile ignition. Then, an edge of the irregular particle is suddenly exposed in a hot gas stream without a

surrounding volatile flame. This exposed edge is directly heated by the surrounding hot gas. The different rotational motions between a particle and volatile flame can change the datum of irregular objects. Sequentially, the opposite edge of the particle is rapidly ignited and char combustion is extended over the surface since the volatile flame shrinks as a function of the residence time. This earlier overlapping combustion and a fast devolatilisation at high temperature and a rapid heating rate enhance the thermal stress and internal pressure inside the particle, leading to a high probability of fragmentation. Only coffee waste particles occasionally experience this phenomenon for oxygen concentrations over 30% and in the size range of 150–255 μm.

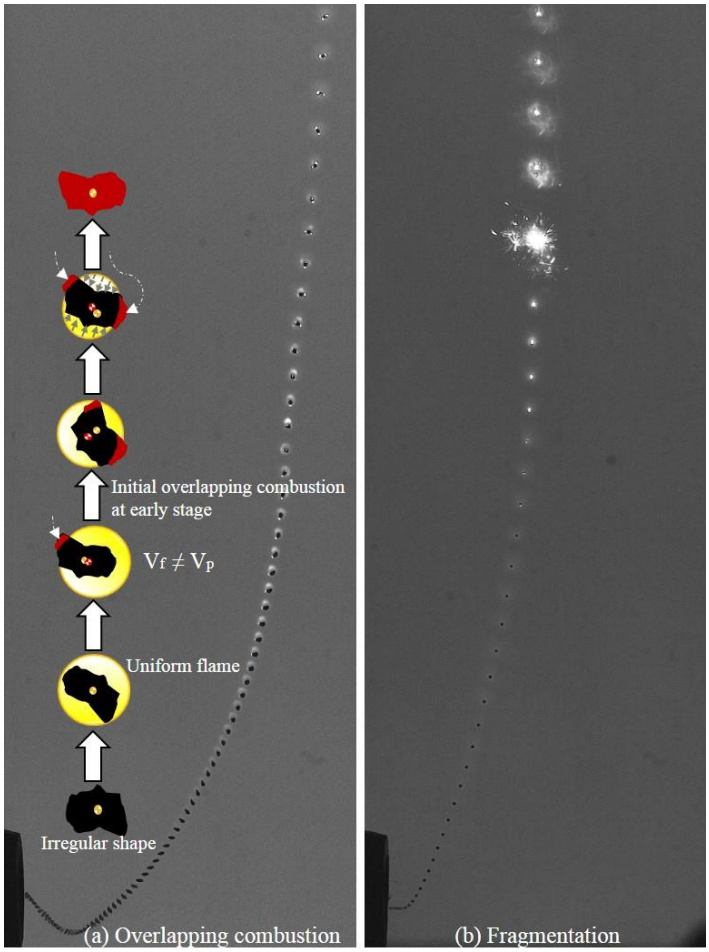

Figure 20. Overlapping combustion and fragmentation occurring in the coffee waste

557 particle.
558
559 *Trajectories of small to large biomass particles for optimisation of burnout*

560 The particle size of biomass is expected to be larger than that of coal for pulverised
561 combustion because of its low density and fast reaction rate. However, large particles injected
562 into a burner can be incompletely burned as they may drop to the bottom of the furnace
563 without combustion. Hence, determination of the particle size for complete burning is
564 essential to achieve a high level of utilisation for pulverised combustion. Saastamoinen et al.
565 [17] also analysed the possible trajectory of particles to be burned virtually and suggested an
566 optimised particle-size for biomass. Fig. 21 shows clearly how realistic trajectories of
567 biomass particles in the cross-sectional configuration develop with regard to size variation.
568 From this, the maximum particle size that can be completely burned is suggested
569 experimentally. Small particles, which range from 150 to 255 μm in diameter, move in the
570 direction of the hot gas stream, regardless of gravity force, as particle velocity increases.
571 Particles of 355–425 μm drop to the bottom of the furnace and are then lifted toward the top
572 due to buoyancy and drag forces as particle mass decreases. However, particles of 425–500
573 μm occasionally drop to the bottom without volatile combustion. Most particles over 500 μm
574 do not burn in the visualisation field because of excessive particle mass and non-mass
575 reduction in the experiment under particular environment conditions. Karampinis [47] also
576 reported that high volumes of particles may go down to the hopper region, where these
577 particles burn without upward movement.

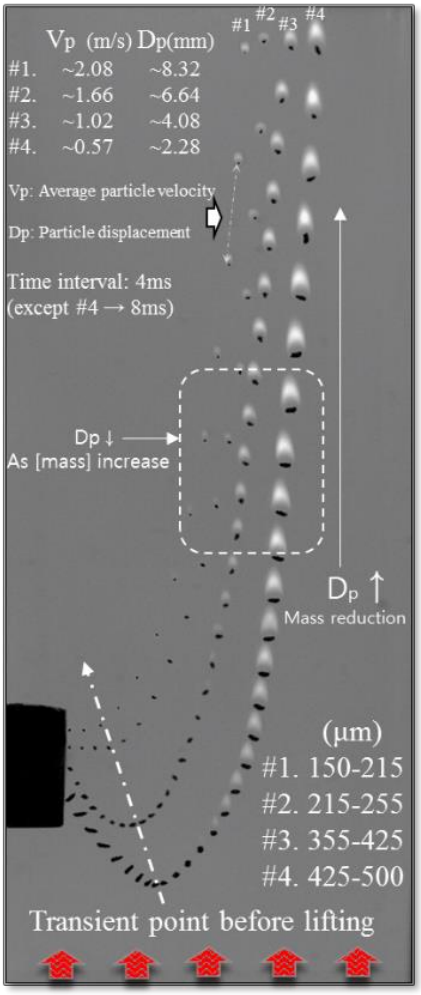

a) Trajectories of burning particles

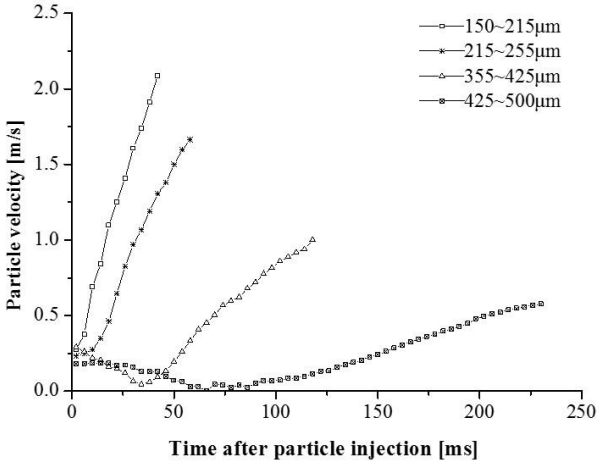

b) particle velocity

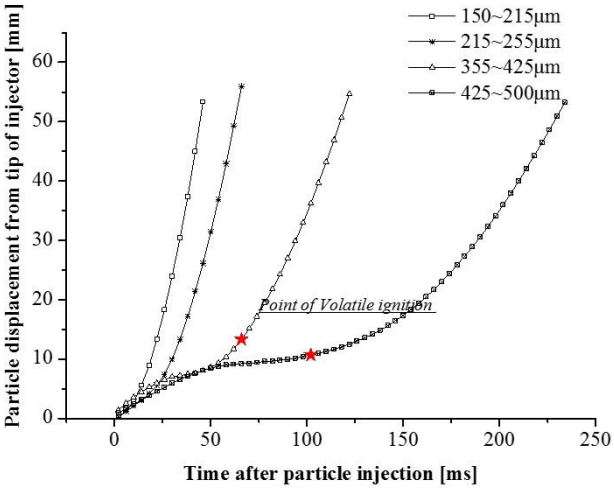

c) Particle displacement

578 Figure 21. Trajectories of small to large biomass particles for burnout, particle velocity and
579 displacement in the combustion process.

580 ## Conclusion

581 Different burning characteristics of disparate biomass particles were observed because of
582 differing chemical and physical properties. These observations were carried out in a
583 laboratory-scale entrained flow reactor with cross jet injection using a high speed camera.

584 Combustion behaviours of biomass particles have been analysed as a function of time and
585 characterised in terms of the effects of oxygen concentration, particle size, particle
586 temperature and other environmental conditions. Also, this study was focused on a
587 measurement of the effective size of the flame over the particle with its intensity to clarify its
588 flame stability along with supporting the modelling description.
589
590 Observation of burning particles shows that flame volatility is not only highly related to the
591 particle's volatile matter content, but is also attributed to soot formation. Biomass has a
592 relatively more volatile content than coal and yields a less sooty flame, but a stable flame is
593 detected for torrefied wood even at the smallest pulverised particles of size 150–215 μm.
594 However, coffee waste requires larger size of over 255 μm to obtain a flame profile
595 equivalent to that of torrefied wood. Sewage sludge in the same size group as other biomass
596 particles has a highly transparent volatile or invisible flame with a longer ignition delay. The
597 initial volatile ignition of the three biomass particle types occurs differently, as these
598 processes are dominantly determined by their compositions, and different effective radii for
599 the volatile flames are observed for each particle.

600 Coffee waste and sewage sludge particles in the size range of 155–215 μm undergo char
601 combustion at an early stage and form a flame with low-soot content. This increases particle
602 temperature rapidly and enables a shorter devolatilisation duration compared with torrefied
603 wood. Also, these particles have thin or invisible flame, and scattered volatile flames are
604 detected at high oxygen concentration from the direct observation. To achieve relatively a
605 soot flame, biomass particles are required to be larger but, the size of pulverised particle is
606 limited due to a probability of unburned particles.

607 The determination of particles size is essential to achieve complete particle burnout in

pulverised combustion. From the experimental results, particles with diameters of 150-255 μm, exposed to a hot gas stream with the studied parameters, move in the direction of the vertical stream, regardless of gravity force. The particle size group of 425–500 μm occasionally falls to the bottom to be incompletely burned without any apparent mass reduction. Consequently, the maximum size of particle that can be burned completely at 1,340 K is in the size range of 355–425 μm. From this result, the optimal biomass particle size would be suggested for a large-scale combustion furnace.

Acknowledgments

The authors gratefully acknowledge support from the Korea Advanced Institute of Science and Technology (KAIST) and the Brain Korea 21+ project. Furthermore, we also thank the effort of Jae Young Yoo, Korea Institute of Energy Research, and who actively contributed in sample preparation.

629

630 **References**

631 [1] Solomon, P. R., et al. (1993). "Progress in coal pyrolysis." Fuel 72(5): 587-597.
632 [2] Kobayashi, H., et al. (1977). "Coal devolatilization at high temperatures." Symposium
633 (International) on Combustion 16(1): 411-425.
634 [3]Li, J., et al. (2014). "High-temperature rapid devolatilization of biomasses with varying
635 degrees of torrefaction." Fuel **122**: 261-269.
636 [4] Bejarano, P. A. and Y. A. Levendis (2008). "Single-coal-particle combustion in O2/N2
637 and O2/CO2 environments." Combustion and Flame 153(1–2): 270-287.
638 [5] Khatami, R. and Y. A. Levendis (2016). "An overview of coal rank influence on ignition
639 and combustion phenomena at the particle level." Combustion and Flame 164: 22-34.
640 [6] Demyirbas, A. (2003). "Hydrocarbons from Pyrolysis and Hydrolysis Processes of
641 Biomass." Energy Sources 25(1): 67-75.
642 [7] Momeni, M., et al. (2013). "Experimental Study on Effects of Particle Shape and
643 Operating Conditions on Combustion Characteristics of Single Biomass Particles." Energy &
644 Fuels 27(1): 507-514.
645 8] Barnes, D. I. (2015). "Understanding pulverised coal, biomass and waste combustion – A
646 brief overview." Applied Thermal Engineering 74: 89-95.
647 [9] Li, J., et al. (2015). "Characterization of biomass combustion at high temperatures based
648 on an upgraded single particle model." Applied Energy 156: 749-755.
649 [10] Balat, M. and G. Ayar (2005). "Biomass Energy in the World, Use of Biomass and
650 Potential Trends." Energy Sources 27(10): 931-940.
651 [11] Lu, H. and L. L. Baxter (2011). Biomass Combustion Characteristics and Implications
652 for Renewable Energy. Solid Biofuels for Energy. P. Grammelis, Springer London: 95-121.
653 [12] Raveendran, K. and A. Ganesh (1996). "Heating value of biomass and biomass pyrolysis
654 products." Fuel 75(15): 1715-1720.
655 [13] Riaza, J., et al. (2014). "Combustion of single biomass particles in air and in oxy-fuel
656 conditions." Biomass and Bioenergy 64: 162-174.
657 [14] Momeni, M., et al. (2013). "Comprehensive Study of Ignition and Combustion of Single
658 Wooden Particles." Energy & Fuels 27(2): 1061-1072.
659 [15] Bharadwaj, A., et al. (2004). "Effects of Intraparticle Heat and Mass Transfer on
660 Biomass Devolatilization: Experimental Results and Model Predictions." Energy & Fuels
661 18(4): 1021-1031.
662 [16] Gera, D., et al. (2002). "Effect of Large Aspect Ratio of Biomass Particles on Carbon
663 Burnout in a Utility Boiler." Energy & Fuels 16(6): 1523-1532.
664 [17] Saastamoinen, J., et al. (2010). "Burnout of pulverized biomass particles in large scale
665 boiler – Single particle model approach." Biomass and Bioenergy 34(5): 728-736.
666 [18] Biagini, E., et al. (2009). "Characterization of high heating rate chars of biomass fuels."
667 Proceedings of the Combustion Institute 32(2): 2043-2050.
668 [19] McLean, W. J., et al. (1981). Direct observations of devolatilizing pulverized coal
669 particles in a combustion environment. Symposium (International) on Combustion 18(1):
670 1239-1248.
671 [20] Khatami, R., et al. (2012). "Combustion behavior of single particles from three different
672 coal ranks and from sugar cane bagasse in O_2/N_2 and O_2/CO_2 atmospheres." Combustion and
673 Flame 159(3): 1253-1271.
674 [21] Yin, C., et al. (2003). "Modelling the motion of cylindrical particles in a nonuniform

675 flow." Chemical Engineering Science 58(15): 3489-3498.
676 [22] Shaddix, C. R. and A. Molina (2009). "Particle imaging of ignition and devolatilization
677 of pulverized coal during oxy-fuel combustion." Proceedings of the Combustion Institute
678 32(2): 2091-2098.
679 [23] Shaddix, C. R., "Correcting Thermocouple Measurements for Radiation Loss: A Critical
680 Review," Proceedings of the 33rd National Heat Transfer Conference, Albuquerque, New
681 Mexico (1999).
682 [24] Lee, H. and S. Choi (2015). "An observation of combustion behavior of a single coal
683 particle entrained into hot gas flow." Combustion and Flame 162(6): 2610-2620.
684 [25] Lee, H. and S. Choi (2016). "Motion of single pulverized coal particles in a hot gas flow
685 field." Combustion and Flame **169**: 63-71.
686 [26] Demirbas, A. (2004). "Combustion characteristics of different biomass fuels." Progress
687 in Energy and Combustion Science 30(2): 219-230.
688 [27] Yang, H., et al. (2007). "Characteristics of hemicellulose, cellulose and lignin pyrolysis."
689 Fuel 86(12–13): 1781-1788.
690 [28] Howard, J. B. and R. H. Essenhigh (1966). "Combustion mechanism in pulverized coal
691 flames." Combustion and Flame 10(1): 92-93.
692 [29] Choi, S. and C. H. Kruger (1985). "Modeling coal particle behavior under simultaneous
693 devolatilization and combustion." Combustion and Flame 61(2): 131-144.
694 [30] Saastamoinen, J. J., et al. (1993). "Simultaneous pyrolysis and char combustion." Fuel
695 72(5): 599-609.
696 [31] Midkiff, K. C., et al. (1986). "Stoichiometry and coal-type effects on homogeneous vs.
697 Heterogeneous combustion in pulverized-coal flames." Combustion and Flame 64(3): 253-
698 266.
699 [32] Gururajan, V. S., et al. (1988). "The combustion of evolved volatile matter in the vicinity
700 of a coal particle—An evaluation of the diffusion limited model." Combustion and Flame
701 72(1): 1-12.
702 [33] Timothy, L. D., et al. (1982). "Nineteenth Symposium (International) on Combustion
703 Characteristics of single particle coal combustion." Symposium (International) on
704 Combustion 19(1): 1123-1130.
705 [34] Kuo, J. T. and C.-L. Hsi (2005). "Pyrolysis and ignition of single wooden spheres heated
706 in high-temperature streams of air." Combustion and Flame 142(4): 401-412.
707 [35] Tyler, R. J. (1980). "Flash pyrolysis of coals. Devolatilization of bituminous coals in a
708 small fluidized-bed reactor." Fuel 59(4): 218-226
709 [36] Viskanta, R. and M. P. Mengüç (1987). "Radiation heat transfer in combustion systems."
710 Progress in Energy and Combustion Science 13(2): 97-160.
711 [37] Fletcher, T. H., et al. (1997). "Soot in coal combustion systems." Progress in Energy and
712 Combustion Science 23(3): 283-301
713 [38] Sivathanu, Y. R. and G. M. Faeth (1990). "Temperature / soot volume fraction
714 correlations in the fuel-rich region of buoyant turbulent diffusion flames." Combustion and
715 Flame 81(2): 150-165.
716 [39] Timothy, L. D., et al. (1988). "Soot formation and burnout during the combustion of
717 dispersed pulverized coal particles." Symposium (International) on Combustion 21(1): 1141-
718 1148.
719 [40] Molina, A. and C. R. Shaddix (2007). "Ignition and devolatilization of pulverized
720 bituminous coal particles during oxygen/carbon dioxide coal combustion." Proceedings of the
721 Combustion Institute 31 II: 1905-1912.
722 [41] Sibulkin, M. (1973). "Estimates of the Effect of Flame Size on Radiation from Fires."

723 Combustion Science and Technology 7(3): 141-143.
724 [42] Di Blasi, C. (1997). "Influences of physical properties on biomass devolatilization
725 characteristics." Fuel 76(10): 957-964.
726 [43] Kanury, A. M. (1994). "Combustion Characteristics of Biomass Fuels." Combustion
727 Science and Technology 97(4-6): 469-491.
728 [44] (2014). Combustion of Pulverised Coal in a Mixture of Oxygen and Recycled Flue Gas.
729 Combustion of Pulverised Coal in a Mixture of Oxygen and Recycled Flue Gas. D. D.
730 Toporov. Boston, Elsevier: i.
731 [45] Küçük, A., et al. (2003). "A study of spontaneous combustion characteristics of a Turkish
732 lignite: particle size, moisture of coal, humidity of air." Combustion and Flame 133(3): 255-
733 261.
734 [46] Holtmeyer, M. L., et al. (2013). "The Impact of Biomass Cofiring on Volatile Flame
735 Length." Energy & Fuels 27(12): 7762-7771.
736 [47] Karampinis, E., et al. (2012). "Numerical investigation Greek lignite/cardoon co-firing
737 in a tangentially fired furnace." Applied Energy 97: 514-524.
738
739
740
741
742
743
744
745